Postprint

Published in *Composites Science and Technology, vol 201, 108504, 2021*

DOI: https://doi.org/10.1016/j.compscitech.2020.108504

Toughening mechanisms responsible for excellent crack resistance in thermoplastic nanofiber reinforced epoxies through in-situ optical and scanning electron microscopy

Lode Daelemans[1], Olivier Verschatse[1], Lisa Heirman[1], Wim Van Paepegem[1], and Karen De Clerck[*1]*

[1] Department of Materials, Textiles and Chemical Engineering (MATCH), Ghent University, Technologiepark 70, B-9052 Zwijnaarde, Belgium

** Karen.DeClerck@UGent.be*

Highlights

* Thermoplastic nanofibers provide excellent toughness to brittle epoxy;

* Specimen design allows in-situ optical and scanning electron microscopy for analyzing the toughening mechanisms in detail;

* Bridging nanofibers behind the crack tip are the main cause of toughness;

* Epoxy failure mode becomes more stable when toughened with nanofibers;

* The developed method can be utilized to determine nanofiber/matrix adhesion as well;

Abstract

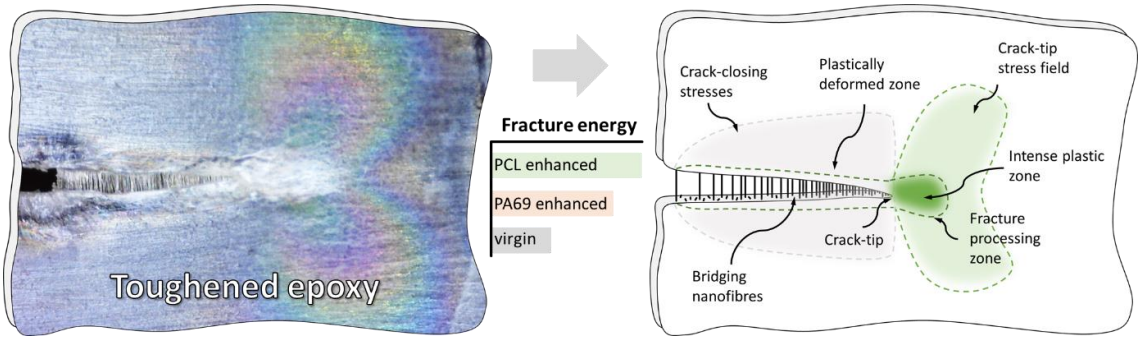

Epoxy is a material of choice for demanding applications thanks to its high chemical stability, stiffness, and strength. Yet, its brittle fracture behavior is an important downside for many sectors. Here, we show that the addition of electrospun thermoplastic nanofibers is a viable toughening strategy to design nanofiber reinforced epoxy materials with excellent toughness. Moreover, the use of transparent film-like specimens allowed in-situ imaging during mechanical testing. Optical and scanning electron microscopy, digital image correlation and crack length measurements are used to analyze the toughening mechanisms responsible for high toughening efficiency in detail. The addition of polyamide and polycaprolactone nanofibers resulted in an increased plastic energy uptake up to 100%. In-situ observation of the crack tip showed that the main energy-absorbing

mechanism was due to bridging nanofibers. There was a profound decrease in toughening efficiency when nanofibers lacked sufficient adhesion with the matrix only when they were oriented parallel with the crack growth direction. The profound understanding of such underlying mechanisms opens up material design in applications where high toughness is required like adhesives, coatings, and fiber-reinforced composite laminates.

Keywords: A. Nano composites, A. Coating, B. Fracture toughness, B. Interfacial strength, C. Damage mechanics, Digital Image Correlation

1. Introduction

One of the main downsides to many (commercial) epoxy polymers used in structural applications is their inherent brittleness, which arises to a large extent from the highly cross-linked network [1]. For example, composite laminates are known to suffer from relatively low delamination resistance which is in part due to the presence of a brittle epoxy rich layer in between the fiber reinforcement plies [2]. In other sectors, epoxy is used as a coating, typically to shield components from moisture, direct contact or electrical charges. Failure of such a coating will not necessarily lead to immediate failure of the component but should be prevented to ensure sufficient lifetime performance of that component. Increasing the toughness of epoxy resins to mitigate brittle fracture would thus benefit a wide variety of sectors.

Different epoxy toughening strategies exist, such as but not limited to, functionalization of the polymer network to include flexible chain segments [3,4], adding rubber or thermoplastic polymer toughening particles [5–7], or the addition of rigid (nano)particles such as clays or graphene flakes [8–12]. Typically improvements in toughness go together with decreases in stiffness and strength, increases in resin viscosity or a decrease in thermal properties.

Recently, the addition of thermoplastic electrospun nanofibers for toughening has gained interest in the research community as they have certain advantages such as fiber morphology and can be made from a wide variety of (polymer) materials [13,14]. Until now, this has predominantly been applied to epoxy-based composite laminates where the nanofibers are easily placed inside the resin-rich interlayer as a nanofibrous non-woven veil [15–24]. Yet, as far as we know, there is almost no research available that investigates thermoplastic nanofiber toughened epoxy itself instead of modified fiber-reinforced composites. Direct analysis of the toughening effect of nanofibers allows underpinning the link between the mechanisms occurring on the microscale and the macroscopically observed fracture toughness. Understanding that link would further allow tuning nanofiber systems towards optimal toughening efficiency. Hence, such insight would be a key component in understanding these novel materials and designing better applications like toughened composite laminates, as well as other epoxy-based materials such as crack-resistant coatings and adhesives.

In our previous work, we analyzed the fracture toughness of nanofiber toughened epoxy through standardized Single Edge Notched Bending (SENB) specimens [14], showing improvements in fracture toughness of an already high toughness resin up to 200 – 300% upon addition of (polycaprolactone) nanofibers. The major downside to this work was that a large number of nanofibrous veils were required to produce the relatively thick specimens. We expect that nanofiber toughened epoxies will be used in applications where the sheet-like morphology of the nanofibrous non-wovens are utilized, and not in (thick) bulk applications. For example, the sheet-like morphology can be exploited in the interlayers of composite laminates [25], but also in thin films or coatings [26–29], and in

adhesive joining of materials [30–32]. In these cases, the nanofibers are not mixed within a resin before processing (which would lead to non-processable viscosities) but rather infused or wetted with resin in their sheet-like form. As such, it would be more interesting, material design-wise, to have relatively thin specimens in accordance with the thickness of a nanofibrous non-woven. This would allow the toughened epoxies to be tested in a manner that will more closely resemble their real-life use, and allow a rapid analysis as specimens will require a lot fewer nanofibers to be made. The latter being especially important for designing new nanofiber types for optimized toughening. Moreover, thin specimens would allow in-situ imaging techniques such as optical or electron microscopy for translucent specimens.

In this work, we provide a direct method to observe and analyze the toughening mechanisms present in nanofiber toughened epoxy. This is enabled through single edge notched tension experiments on thin specimens and in-situ crack observation by optical and scanning electron microscopy. In Section 2, a detailed description of the specimen production and analyzing techniques is given. The work is based on the same materials that we previously investigated for nanofiber toughened composite laminates (e.g. same resin type, same nanofiber types, …) [33–38], yet the approach is generally applicable to other nanofiber/matrix combinations as well. First, the mechanical response based on load-extension data from fracture experiments is analyzed and an approach to numerically define a relevant fracture measure is brought forward (Section 3.1). This fracture measure is required as the limited thickness of the considered fracture specimens excludes a direct measurement of the material's inherent plane strain fracture toughness. Thereafter, a detailed analysis of the toughening mechanisms using in-situ microscopic data, linked to the fracture toughness measure, is used to define the (micro)mechanisms present in the toughened materials (Section 3.2). Using these insights, we extend our analysis to oriented specimens to study the importance of nanofiber-matrix adhesion on the fracture toughness measure (Section 3.3). Finally, we conclude with an overview and short discussion of the toughening mechanisms present in nanofiber toughened epoxy and their relation to design optimally toughened materials (Section 3.4).

2. Experimental

2.1. Materials

Polyamide 6.9 (PA69, Scientific Polymer Products, M_w 58 000 g mol^{-1}), polycaprolactone (PCL, Sigma Aldrich, M_n 80 000 g mol^{-1}), formic acid (Sigma Aldrich, 98%), and acetic acid (Sigma Aldrich, 98%) were used as received for the electrospinning solutions. Epoxy resin and hardener (Momentive, EPIKOTE MGS RIMR135 + EPIKURE MGS RIMH137) were used as received and based on a standard diglycidyl ether of bisphenol A (DGEBA) epoxy resin and an amine type curing agent.

2.2. Electrospinning of nanofibrous veils

Nanofibrous veils of homogeneous areal density (here 9 – 10 g m^{-2}) were electrospun on an in-house developed multi-nozzle setup as described in [24]. The electrospinning conditions for PA69 nanofibers are reported in [24], those for PCL nanofibers are reported in [38].

2.3. Production of nanofiber enhanced epoxy films

Nanofiber modified epoxy films were produced by the procedure outlined in **Figure 1**. Briefly, a nanofibrous veil of homogeneous areal density is placed on a flat glass mold surface treated with a release agent. A small amount of epoxy resin is applied to the veil using a syringe which subsequently wets out the nanofibers through wicking. Using a squeegee and a release foil (here vacuum bagging foil) the epoxy is applied evenly onto the nanofibrous veil after which pressure (here 40 kPa) and a temperature program (here 24 hours at 20°C, followed by 15 hours at 80°C, resulting T_g of 85 – 90°C and approximate cross-link density of 1500 mol m^{-3} [39,40]) are applied for curing. This resulted in thin nanofiber modified epoxy films (here a nominal thickness of 100 µm). Specimens were cut from this film in the required dimensions and placed in a dedicated notching mold. This mold consists of two pieces of 3 mm thick polycarbonate machined to the required specimen dimensions with a milled notch of a certain length. The notching mold ensures that a reproducible notch can be applied using a (new) microtome blade (blade thickness 250 µm, blade tip radius 5 µm) for Single Edge Notch Tension (SENT) experiments. Non-modified virgin epoxy SENT specimens are made in the same manner, except without the application of a nanofibrous veil in the first step.

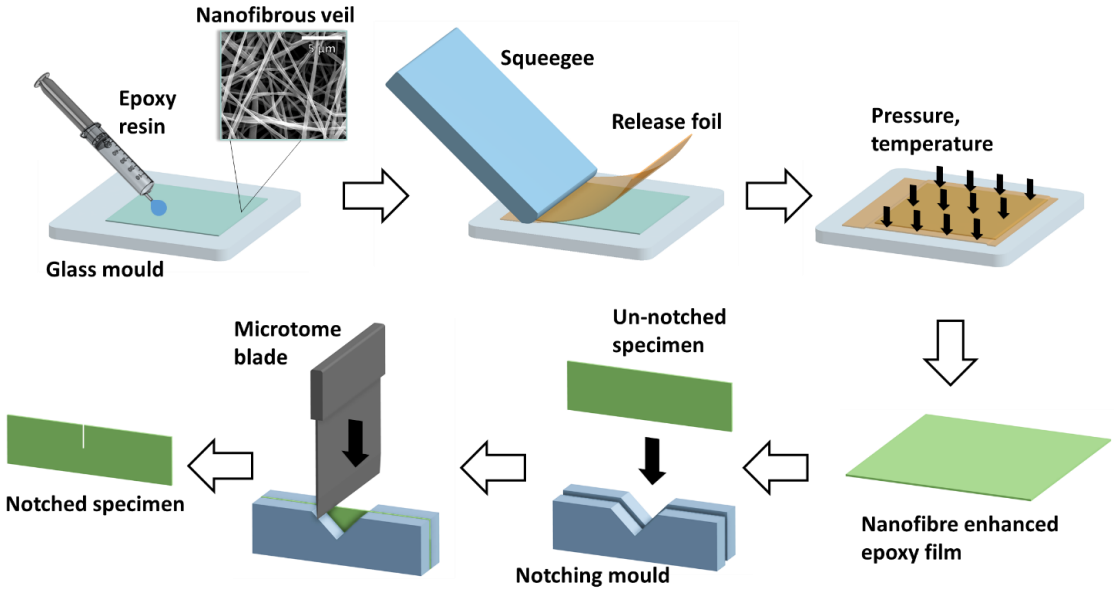

Figure 1 – Schematic view of the production route used to obtain thin nanofiber modified epoxy SENT specimens.

2.4. Single Edge Notch Tension experiments

An example of the produced nanofiber modified SENT specimens is shown in **Figure 2a** and has nominal dimensions of 40 x 5 x 0.1 mm^3 and a nominal gauge length of 20 mm. The specimens remain transparent upon the addition of nanofibers, making the nanofiber reinforced epoxy well suited for coating or optical applications. Care was taken to produce specimens with a thickness in the same order of magnitude (here a nominal thickness of 100 µm) as to minimize any effect on the stress state at the crack tip between specimens due to non-plane strain crack growth conditions. These specimens are loaded in tension on a Dynamical Mechanical Analyzer instrument (TA Instruments Q800 DMA) in 'static testing mode' at 0.1 mm min^{-1}. Displacement and load are recorded during the SENT experiment while in-situ microscopic images are recorded at a frequency of 1 Hz using a long working distance USB microscope (Dino-Lite AM73915MZTL) to monitor the crack growth (**Figure 2b**). Additionally, a similar

experiment was performed within an in-situ scanning electron microscope environment (Phenom XL, Phenom 150 N tensile stage). To visualize the strain fields in the specimens, Digital Image Correlation (DIC) is performed. A speckle pattern was applied to several specimens using matt white and black spray-paint through an airbrush (**Figure 2c**). The strain fields are determined using GOM Correlate (30 pixels subset, 5-pixel mesh point distance). Analysis of rigid body translations of a speckled specimen showed an acceptable noise level of $\mu = 0.00\%$ and $\sigma = 0.021\%$ on the calculated strain fields. As the speckle pattern had a thickness of ± 10 µm, compared to the 100 µm of the specimen, it slightly affected the recorded load, and thus, for those tests, the recorded load is not considered.

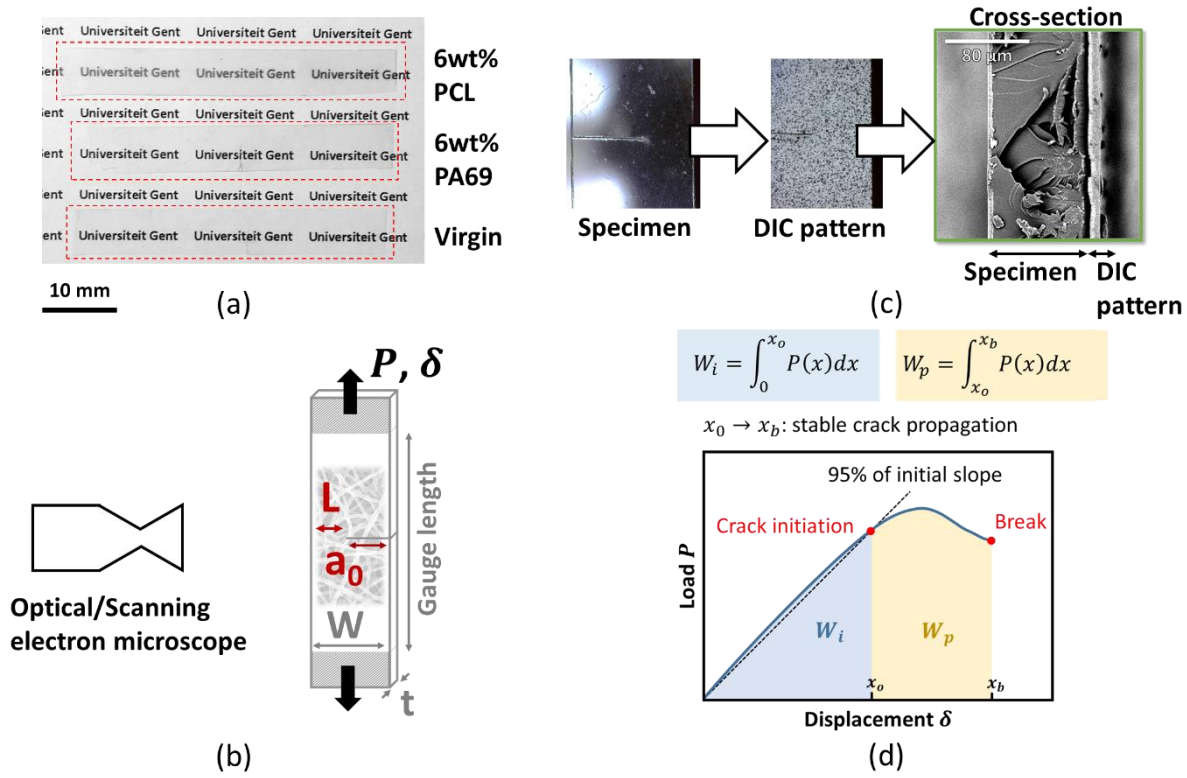

Figure 2 – (a) Several SENT specimens produced as outlined in Figure 1 on background text to show their transparency (red dotted lines were added to situate the specimens). (b) Schematic view of the test setup with in-situ microscopic measurement during tensile testing of the SENT specimens with an initial crack of length $\boldsymbol{a_0}$ and remaining ligament length $\boldsymbol{L}$. (c) Application of a speckle pattern for DIC analysis. The insert shows an SEM image of the cross-section of a speckled specimen. (d) Data reduction scheme to determine the crack initiation and propagation work based on the recorded load-displacement data.

The load-displacement data is used to determine the crack initiation and crack propagation work applied to the specimen during the SENT experiment as represented in **Figure 2d**, similar to the procedure by Yang *et al.* [41]. The crack initiation work W_i is defined as the amount of area underneath the load-displacement curve up to displacement x_0 which corresponds to the intersection between the curve and a straight line with a slope equal to 95% of the initial slope. In-situ microscopy showed that this point coincided with the onset of crack initiation. Similarly, the crack propagation work W_p is defined as the amount of area underneath the curve from x_0 to the displacement at break x_b (stable crack growth). As the amount of work is dependent on the ligament length L, i.e. $L = W - a_0$,

and the thickness t, we define the crack initiation and propagation energy, E_i and E_p respectively, as in **Equation 1**.

$$E_i = W_i/(Lt) \text{ , and, } E_p = W_p/(Lt) \quad \text{(Eq. 1)}$$

The total energy for fracture E_{tot} of the specimens is the sum of both contributions, as in **Equation 2**.

$$E_{tot} = E_i + E_p \quad \text{(Eq. 2)}$$

3. Results and discussion

3.1. Analysis of the toughening effect through the work of fracture of SENT specimens

Figure 3a shows a representative load-displacement curve for a non-modified virgin epoxy, a 6wt% PA69 and a 6wt% PCL nanofiber modified epoxy SENT specimens (a/W = 0.5). Immediately, one can see that the addition of nanofibers results in a larger "plastic deformation" region on the load-displacement curves, corresponding to a longer stable crack progression. This indicates the potential for nanofibers to reduce the brittle non-stable fracture behavior of epoxies. As expected, the introduction of (less stiff) thermoplastic nanofibers slightly lowers the stiffness of the epoxy films as visible by the lower slope of the load-displacement curve in the elastic region of the modified SENT specimens. This decrease, which is around 5% compared to the non-modified specimens, is well acceptable for the majority of epoxy applications (composites, coatings, …).

The difference in crack initiation energy E_i between the virgin and the nanofiber modified specimens (a/W = 0.5, 6wt% nanofibers) was not statistically significant (**Figure 3b**, two-tailed T-test, α = 0.05, smallest p-value 0.38). This thus indicates that the energy required for crack initiation remains similar between modified and non-modified specimens. The crack propagation energy E_p shows a completely opposite trend where the addition of nanofibers to the epoxy results in a huge increase in energy take-up of about 180% for 6wt% PA69 and 200% for 6wt% PCL (**Figure 3c**, two-tailed T-test, α = 0.05, largest p-value 0.0008). This shows that the majority of the toughening occurs during stable crack growth in the nanofiber modified specimens.

The results of the SENT experiments thus show the effectiveness of these nanofibers for toughening epoxy resin as even a small amount of nanofibers already results in big improvements of the energy required for fracture thanks to an extended stable crack propagation phase. For example, the total fracture energy increases from 3365 J m^{-2} for the virgin specimens to 4500 J m^{-2} and even 4980 J m^{-2} for 6wt% PA69 and 6wt% PCL nanofiber toughened specimens respectively at a/W=0.5. The amount of fracture energy taken up during both crack initiation and propagation is directly related to the inherent fracture toughness of the material. **Figure 3d-f** shows that the total fracture energy of nanofiber toughened specimens increases compared to the non-toughened epoxy for a whole range of ligament lengths (statistically significant, one-tailed T-test, α = 0.05, largest p-value 0.005). This due to a higher crack propagation energy for nanofiber toughened specimens, with PCL nanofibers being more effective than PA69 nanofibers (statistically significant, one-tailed test, α = 0.05, p-value 0.0004).

These data could enable the use of the essential work of fracture work (EWF) method to determine the inherent fracture toughness of the materials. However, this method is mainly applied to ductile polymer film materials [40,42–44]. According to the EWF method, SENT experiments are performed over a range of ligament lengths to extrapolate

the total work of fracture (elastic and plastic energy take-up) towards a zero ligament length, which is a measure for the inherent fracture toughness. In the case of our (nanofiber toughened) epoxy films however, this approach is not feasible. First of all, the specimens did not show full ligament yielding before crack growth, one of the conditions for the EWF method to be valid. Moreover, a transition from stable (ductile) to non-stable (brittle) crack growth occurred and extrinsic toughening mechanisms were observed for which the energy absorptions depends on the amount of stable crack growth (detailed in Section 3.2). Typically abrupt non-stable failure occurred before the full ligament failed under stable crack growth.

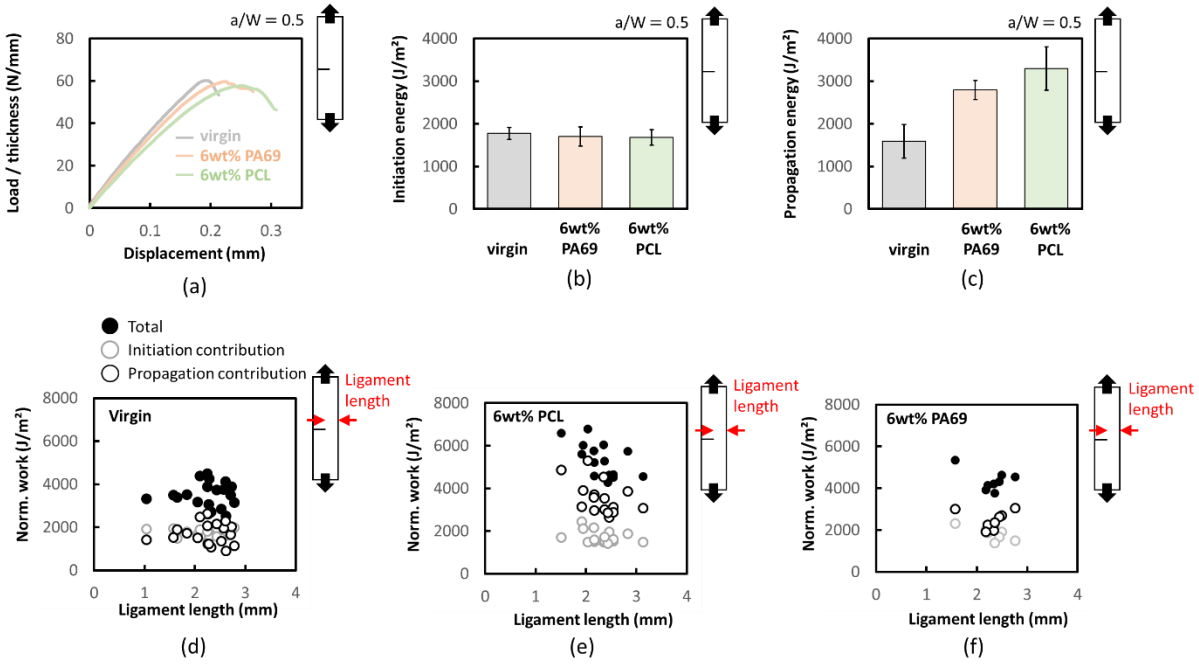

Figure 3 – (a) Representative load-displacement curves for a virgin, 6wt% PA69 and 6wt% PCL nanofiber modified SENT specimen show a slight decrease in the slope of the elastic portion, but a larger plastic region upon addition of nanofibers. (b) Crack initiation and (c) propagation energy show that the propagation energy increases upon the addition of PA69 and PCL nanofibers. (d-f) The total fracture energy, and its initiation and propagation contributions, for virgin and nanofiber modified SENT specimens over a range of ligament lengths. An increase in total fracture energy is noticeable over the whole range upon the addition of nanofibers, especially for 6wt% PCL.

In-situ optical micrographic images allowed to determine the crack growth corresponding to the related load-displacement data points (**Figure 4a-c**). This enables the construction of an *R*-curve by plotting the total energy take-up in function of the crack length as is shown in **Figure 4d** for the same specimens as depicted in Figure 3a-c. Two important insights can be obtained from these *R*-curves. First, the addition of PA69 or PCL nanofibers increases the stable crack growth length before abrupt failure occurs (sub-critical crack growth) from 0.5 mm for the virgin epoxy to approximately 1.0 – 1.5 mm for the 6wt% PA69 and PCL modified epoxy, an increase in stable crack growth length of more than 100%. Secondly, while the amount of the (normalized) work of fracture quickly levels off with increasing crack length for the virgin material, the addition of nanofibers results in a more monotonic increase throughout the stable crack growth regime. Both insights prove that adding electrospun nanofibers is not only an effective and viable toughening strategy, the gradual increase in the amount of energy necessary to progress a crack also results in inherent material safety. Indeed, the rising *R*-curve

indicates that more energy is required (up till a critical point) to progress small cracks further which is unlike the brittle fracture behavior encountered in pristine epoxies.

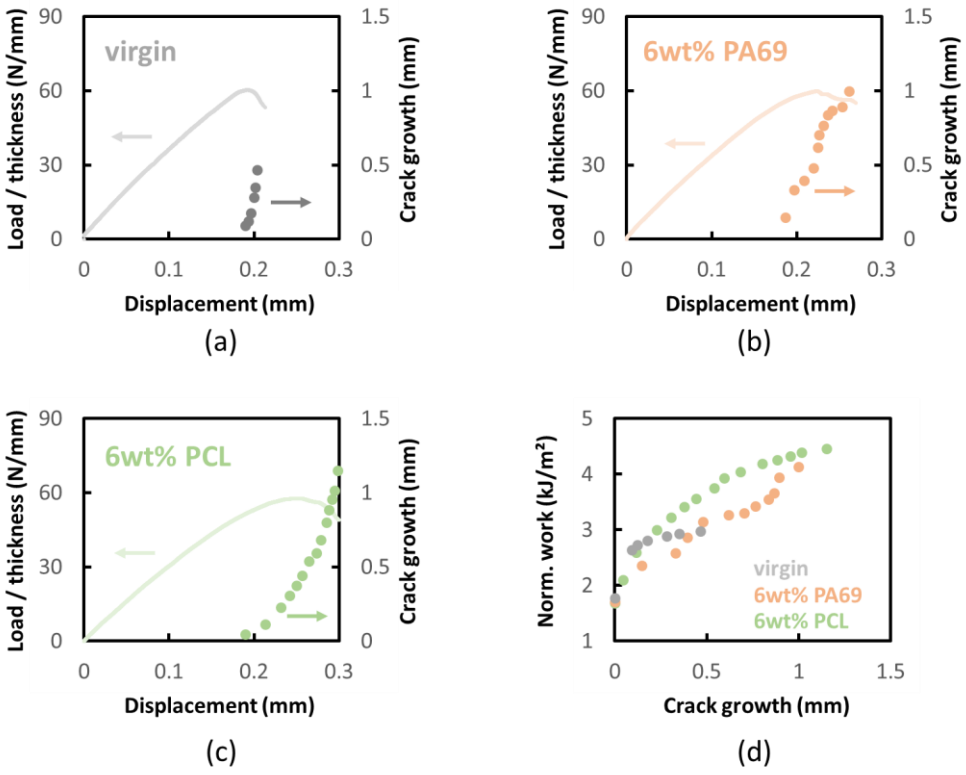

Figure 4 – (a-c) Load-displacement curve and corresponding crack growth-displacement data points measured through in-situ microscopy for the SENT specimens reported in Figure 3a-c. (d) Constructed ***R***-curve based on the load and crack growth data for the three specimens.

The advantage of the thin-film SENT specimens over the Single Edge Notch Bending (SENB) specimens that we used in previous work [14] is that the SENT specimens more closely mimic the actual crack progression in applications like adhesives, coatings and even fiber-reinforced composites. In addition, they are simpler to produce, a lot fewer nanofibers are required (approximately 50 – 100 times less per specimen) and they allow for the addition of in-situ imaging techniques thanks to their translucency (optical microscopy, electron microscopy, digital image correlation, …). Moreover, the obtained values of fracture energy are in close agreement with the strain energy release rate (fracture toughness) reported for the RIMR 135 resin system using standardized SENB specimens: a fracture toughness at crack initiation $G_{Ic,SENB}$ of around 1600 J m^{-2} is obtained in Refs. [14,39,45] for the non-modified virgin epoxy resin through experiments performed according to the ASTM D5045 procedure for determining the plane-strain fracture toughness and strain energy release rate of plastic materials. The crack initiation energy of virgin SENT specimens averages out at 1745 ± 170 J m^{-2} for the range of a/W tested here, and is indeed quite similar to the SENB result.

3.2. Analysis of the toughening micro-mechanisms through in-situ microscopy during SENT testing

The main difference in energy take-up between non-toughened and nanofiber toughened epoxy SENT specimens is in the crack propagation zone of the load-displacement curve

(stable crack growth, Figure 3a). **Figure 5** shows the observed crack tip of virgin epoxy specimens and toughened with 6wt% PA69 and PCL nanofibers during different stages of the SENT experiment. The visual onset of crack growth from the microscopic images coincided with the onset defined from the slope in Figure 2d. At this point, the stress concentration in front of the crack tip resulted in a visually observable fracture processing zone (FPZ) of around 100 – 200 µm in diameter. Upon further loading, the FPZ increases in size and becomes more oval-shaped than circular, with a diameter of around 250 – 500 µm. Interestingly, the FPZ of virgin epoxy specimens looks different than those of nanofiber toughened specimens. While the FPZ of virgin epoxy shows a well-defined notch-like feature at the front, the FPZ of nanofiber toughened specimens looks more homogenous without a clear presentation of this feature, possibly indicative of different (micro)mechanisms in the FPZs. Similarly, while the boundaries of the FPZ are well-defined for the non-toughened virgin material, the FPZ of the nanofiber toughened specimens has a slight color gradient through its boundary. This is especially visible on the images for the 6wt% PCL toughened specimen. In the wake of the crack tip, one can also clearly see a zone of deformed material at the crack edges. Finally, these images clearly show nanofiber toughened specimens had a longer stable crack progression.

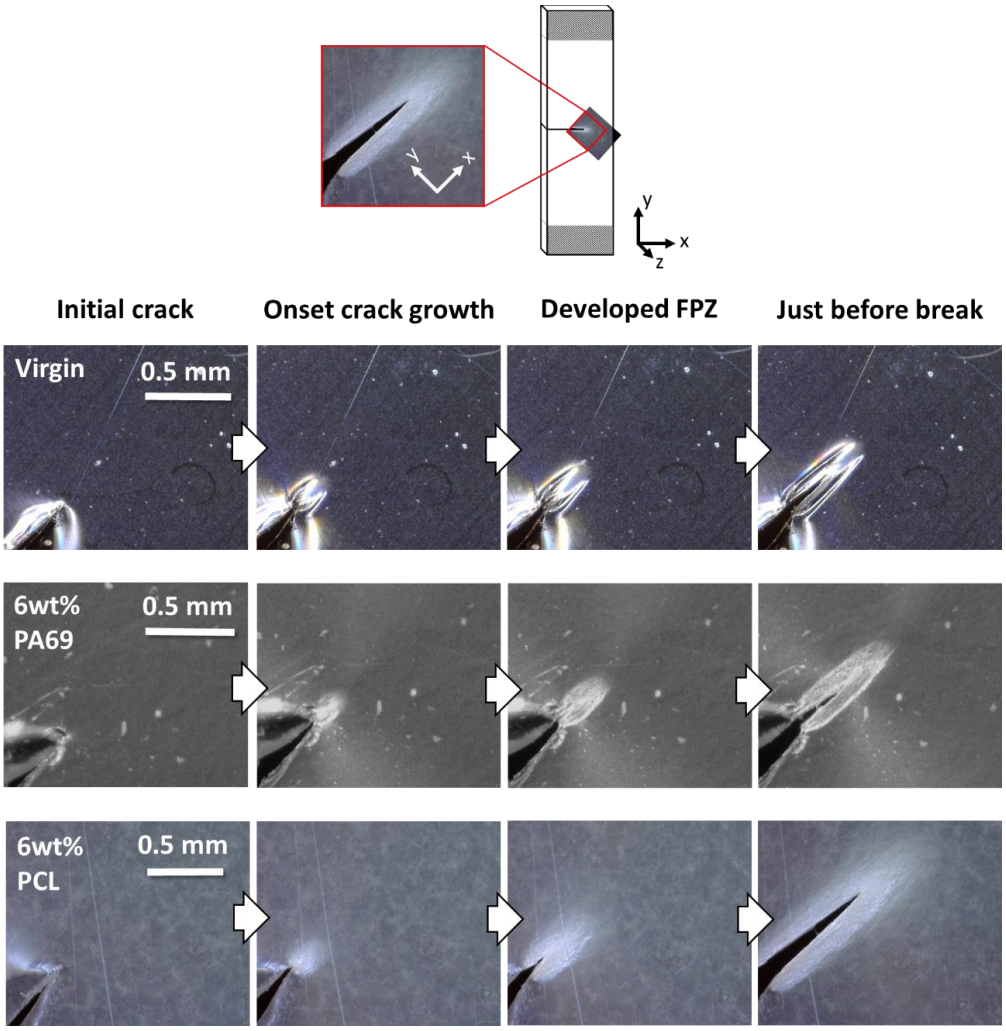

Figure 5 – In-situ microscopic view of the crack tip before and at three distinct stages (onset crack growth, developed fracture processing zone and just before unstable fracture) during the SENT experiment for a virgin and two nanofiber toughened specimens. One can see an overall slightly different appearance of the FPZ in front of the crack tip, as well as in the length of stable crack progression for the nanofiber toughened specimens.

A two-camera setup with a polarized transmission light-source results in an even better view of the mechanisms acting in the nanofiber toughened specimens. This is represented in **Figure 6** and **Video 1** for a 6wt% PCL specimen at two different points in the SENT experiment. The crack tip (A) is seen to remain relatively sharp at a millimeter scale. While the specimens are initially translucent, the fracture processing zone (B) in front of the crack tip becomes opaque, likely due to microscale damage. Similarly, the stressed areas (C) around the crack tip become darker and show a typical color gradient due to polarized light scattering inside the material. The shape of these stress fields is as expected from traditional fracture mechanics.

Upon crack growth, we also observe the development of a nanofiber bridging zone (D) between the two crack halves. This mechanism of nanofiber bridging was pointed out in earlier studies as the main toughening mechanism in nanofiber modified composite laminates, but the proof for its existence was mainly based on post-mortem microscopic imaging of fractured specimens [46]. Here, the use of in-situ microscopy during fracture experiments shows the development of a nanofiber bridging zone during actual fracture for the first time, not only proving that the earlier postulated mechanism is indeed occurring, but it also allows a better understanding and analysis of this toughening mechanism. Throughout crack progression, nanofibers are seen to start bridging crack halves and being stretched. This takes up energy due to the plasticity of the nanofiber polymer (here PCL or PA69). Indeed, one can see that upon crack growth some of the nanofibers are stretched up to their elongation at break (E) after which the elastic energy is released and the nanofibers coil back towards the crack edges. The images further revealed that for PCL and PA69 toughened specimens, the size of the nanofiber bridging zones easily extends towards the millimeter region, even though the nanofibers themselves are on the (sub)micron scale in diameter. This is in agreement with indirect measurements of the nanofiber bridging zone extracted from Mode II delamination tests of nanofiber interleaved composite laminates reported in [33,37].

[VIDEO 1]

VIDEO 1 – Crack initiation and progression in a 6wt% PCL toughened epoxy SENT specimen showing the development of a fracture processing zone in front of the crack tip and a nanofiber bridging zone behind the crack tip. Vibrations are due to manual refocusing through the focus knob on the USB-microscope during filming.

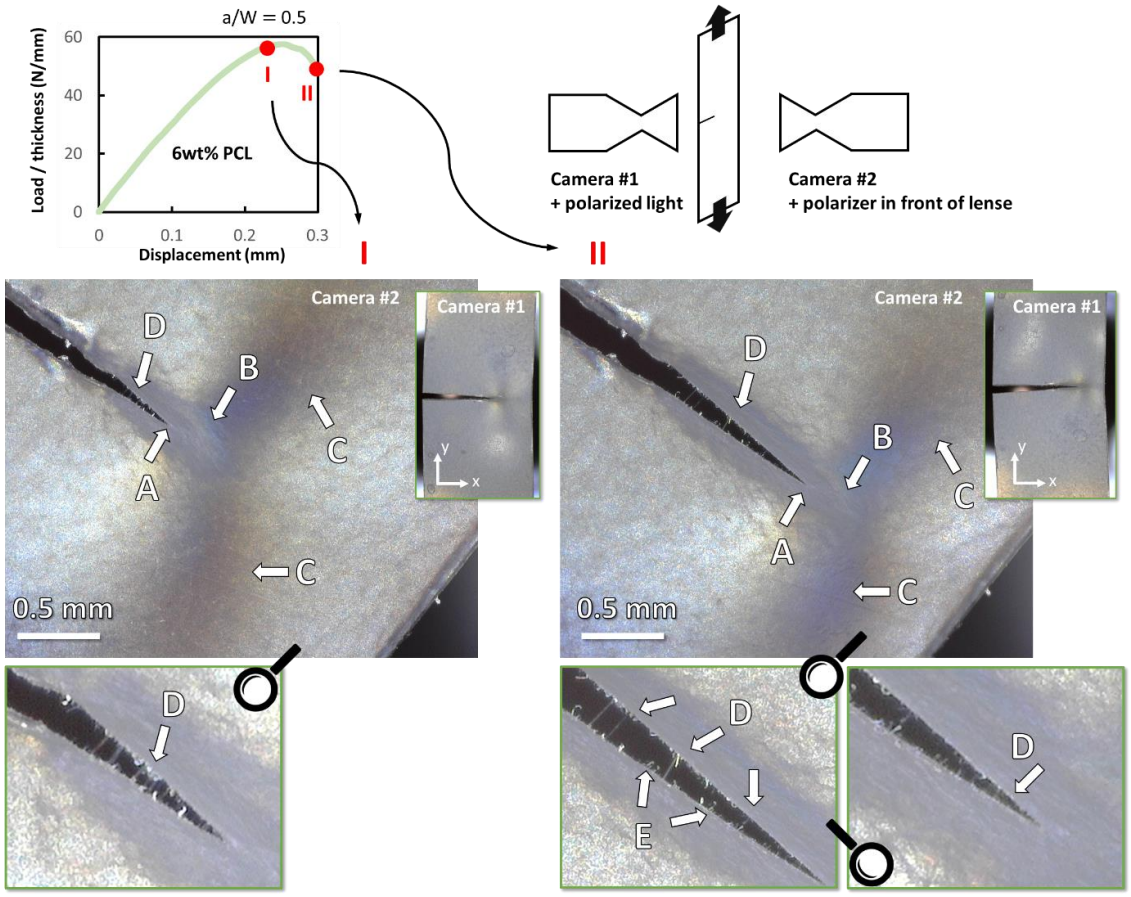

Figure 6 – Crack mechanisms visible through in-situ polarized microscopy during testing of a 6wt% PCL toughened SENT specimen at two different stages (I and II). The white arrows indicate the crack tip (A), the fracture processing zone (B), the crack-tip stress fields (C), bridging nanofibers (D) and broken nanofibers (E).

In-situ scanning electron microscopy, on the other hand, shows that the crack tip remains fairly sharp even at the micrometer scale (**Figure 7a**), similar to the brittle epoxy itself. This is further evidence that the main energy absorption is happening during crack propagation and behind the crack tip (extrinsic toughening) due to bridging nanofibers instead of in front of the crack tip (intrinsic toughening). Furthermore, the SEM image clearly shows the vast amount of actively bridging nanofibers just behind the crack tip. The toughening is in that viewpoint a numbers game as the contribution to energy take-up of a single nanofiber is small, but the total energy take-up is far higher thanks to the high amount of nanofibers in an electrospun nanofibrous veil. For the nanofibers used here, the majority of toughening seems to happen relatively close to the crack tip where most bridging nanofibers are still intact. At further distances away from the crack tip, more broken nanofibers are visible. Post-mortem SEM analysis of the SENT nanofiber toughened specimens (**Figure 7b**) indeed shows many remnants of nanofibers that bridged the crack halves, i.e. nanofibers protruding slightly from the crack surface and long "pieces" of nanofibers laying on the crack surface after they broke. This fracture surface morphology is very similar to what is reported in earlier studies for nanofiber toughened composite laminates, for example in [20,22,35,47]. In addition, the top row images in Figure 7a show that at the micrometer scale, the concept of self-similar crack growth is not completely valid at the crack tip. Small deflections in crack orientation, possibly induced by the extrinsic nanofiber bridging mechanism, and micro-cracking around the crack tip results in a slightly different crack tip view during crack growth. In

comparison, at the "macroscopic" scale such as in Figure 6, the crack tip remains identical throughout the crack growth.

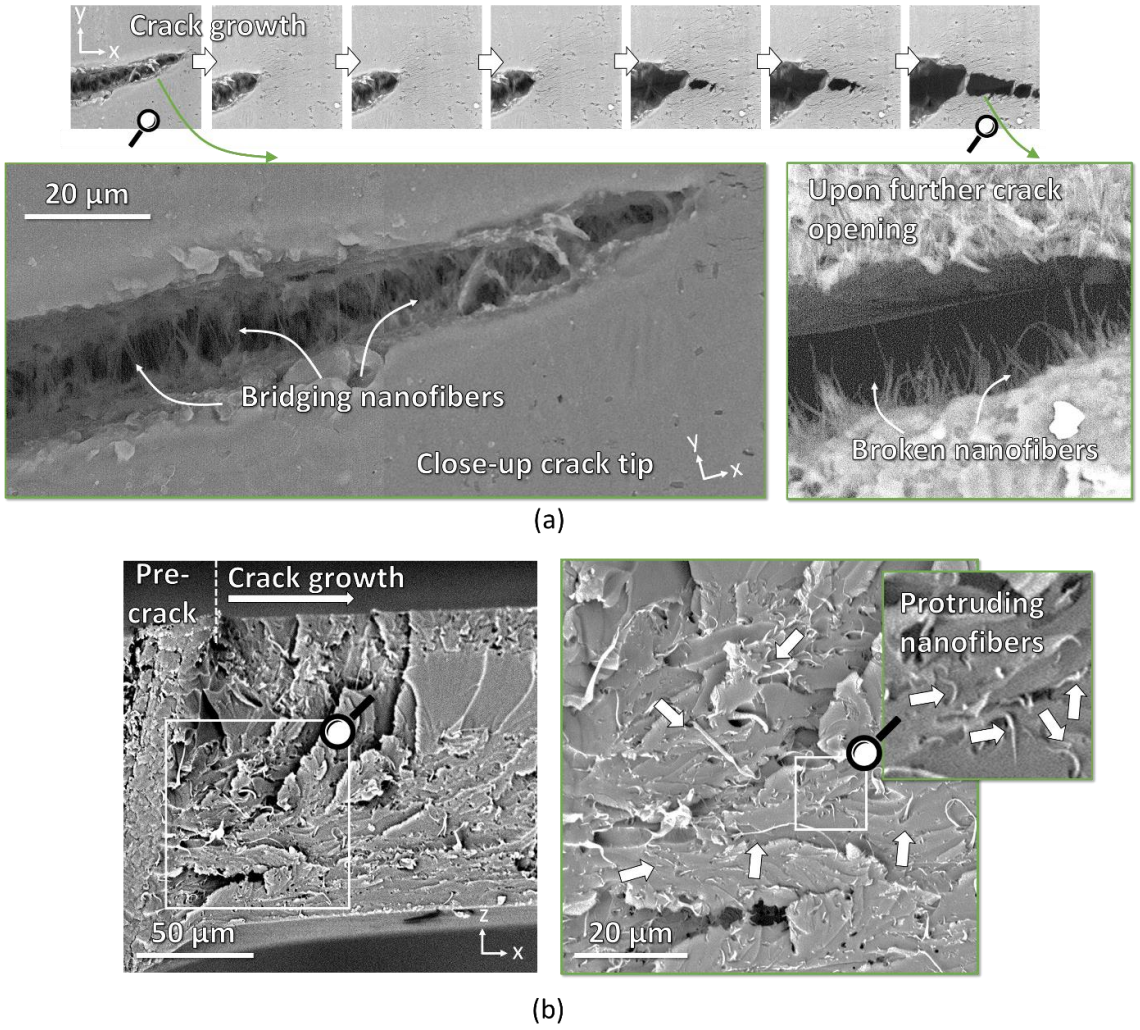

Figure 7 – (a) In-situ SEM images of crack growth in a 6wt% PCL toughened specimen showing many bridging nanofibers acting just behind the relatively sharp crack tip as well as broken nanofibers further away from the crack tip. (b) Post-mortem view shows the remnants of the bridging fibers protruding from the fracture surface.

Figure 8 shows the ε_y strain maps obtained through DIC analysis on a virgin (top) and a 6wt% PCL toughened (bottom) epoxy SENT specimen at the onset of crack growth (left) and just before abrupt failure (right). We know that at the onset of crack growth no substantial toughening is happening yet since the crack initiation energy remains similar for toughened and non-toughened specimens. Comparison of the ε_y strain field indeed shows a similar behavior of both types of specimens as well: a stress concentration field as expected from traditional fracture mechanics. In both cases, i.e. non-toughened and toughened, the maximum strain in front of the crack tip reaches about 2%, after which crack growth starts occurring.

In contrast to this, the strain fields taken just before the abrupt failure of the specimen show a distinct difference between the virgin and toughened specimens. The virgin specimens still have a strain field very similar to that at the onset of crack growth, although with a slightly larger maximum strain in front of the crack tip (more developed

FPZ). The crack progression in the non-toughened specimens thus behaves self-similar. A very different strain field behavior just before break is observed for the 6wt% PCL nanofiber toughened specimen compared to the strain field at the onset of crack growth. Although the typical lobe-sided strain field acting in front of the crack-tip is still visible, there are two additional effects visible (indicated by the white arrows). A much higher strain is reached in the fracture processing zone in front of the crack tip compared to the non-toughened virgin specimen. Maximum strains up to 6% are occurring, indicating a more intense plastic zone. In addition, the strain field in the wake of the crack tip does not relax back to zero strain but instead shows the presence of (relatively low) strains occurring over the whole crack growth zone. From the in-situ microscopy images, we know that in this zone the nanofiber bridging is taking place, with a higher concentration of bridging nanofibers towards the crack tip, as well as some permanent plasticity (induced in the intense plastic zone in front of the crack tip).

Comparing the strain fields between 6wt% PCL and PA69 toughened specimens (**Figure** 9), larger strains are present in the PA69 reinforced specimens (at the same ligament length) for both ε_y (Figure 9a) and ε_{xy} (Figure 9b). For the ε_y-field, the main difference between both specimens is in front of the crack tip, while for the ε_{xy}-field it is behind the crack tip. These differences must be induced by the underlying deformation mechanisms present in the specimens. Since the PCL nanofibers are less stiff and have a higher elongation at break than PA nanofibers [14], one would expect that they result in larger strains. However, we know as well from previous research that PCL nanofibers exhibit excellent adhesion with this epoxy in comparison to PA nanofibers which tend to debond more easily [35,38]. This debonding of PA69 nanofibers in the strain field around the crack tip can explain why we observe larger overall strains at a macroscopic level. Indeed, debonding of the nanofibers within the strained region would reduce their reinforcing effect as well as causing more micro-damage, thus resulting in a more compliant material locally. The importance of the debonding phenomenon is further analyzed and confirmed in **Section 3.3** using specimens made with aligned nanofibers.

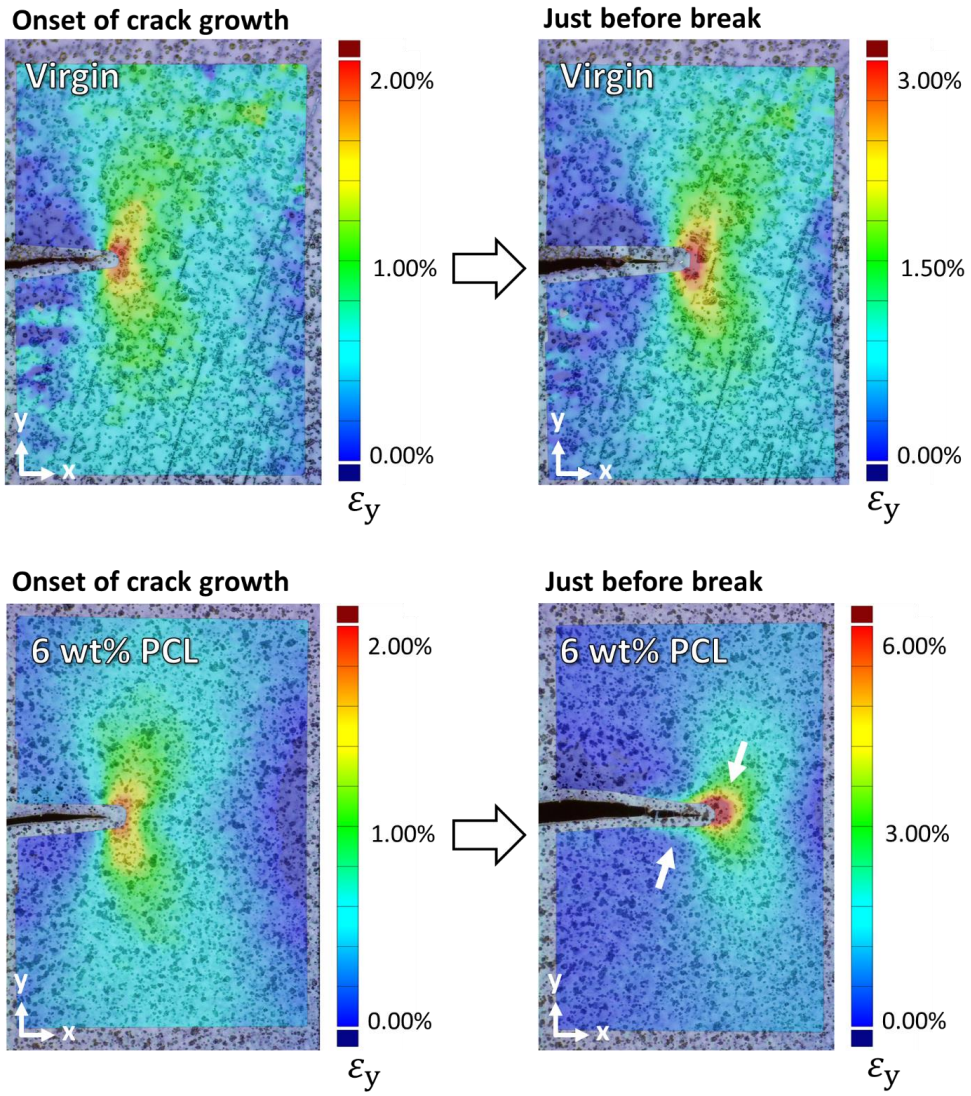

Figure 8 – ε_y strain fields obtained through DIC analysis on a non-toughened (top) and 6wt% PCL nanofiber toughened (bottom) SENT specimen at the onset of crack growth (left) and just before break (right). The strain fields are as expected from a traditional crack tip stress concentration, except in the case of 6wt% PCL just before break (bottom right figure), where a distinctly different field can be observed with higher strains in front of the crack tip and a non-zero strain region in the wake of the crack tip.

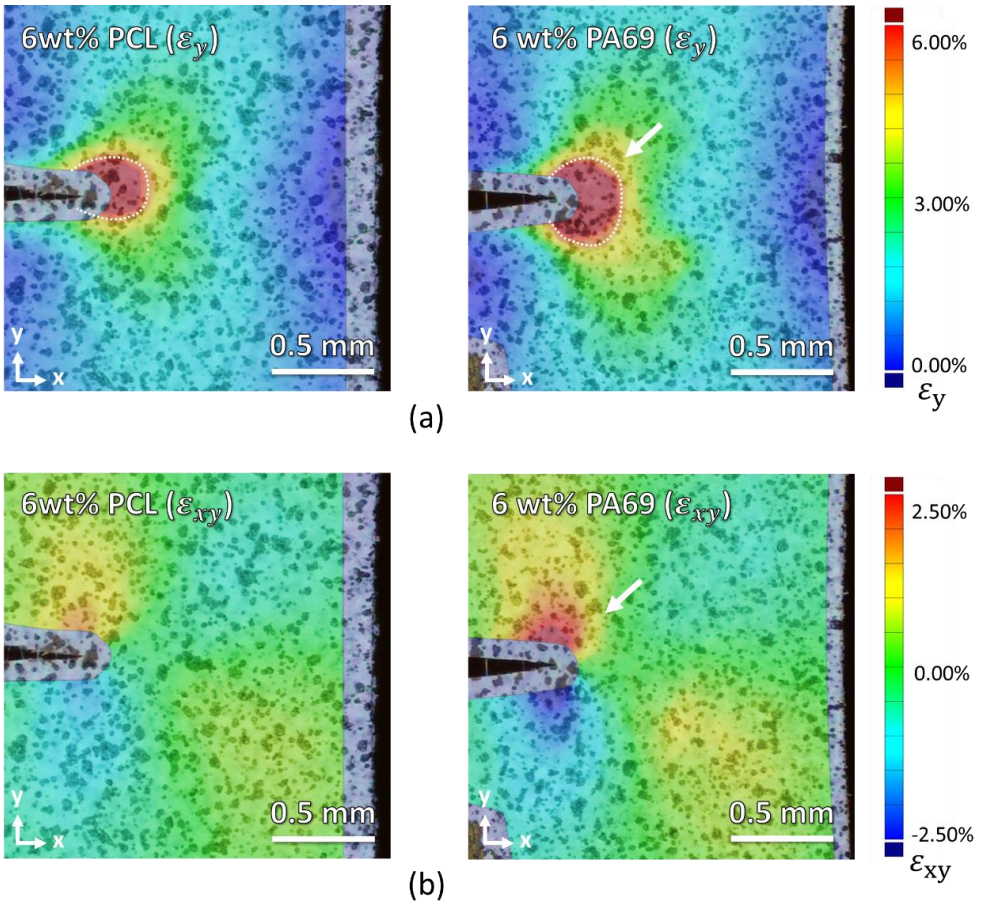

Figure 9 – (a) Zoom of the $\boldsymbol{\varepsilon_y}$-strain field around the crack tip for a 6wt% PCL (left) and PA69 (right) toughened epoxy specimen at the same ligament length show that the general shape of the strain field is similar. The PA69 specimens showed slightly larger strains and a larger strain field in front of the crack tip (dotted lines). (b) Zoom of the $\boldsymbol{\varepsilon_{xy}}$-field (shear strain) for the same specimens as well show larger strains for the PA69 toughened specimens, especially behind the crack tip. These differences in strain fields show that the underlying deformation mechanisms might be different for both nanofiber types.

3.3. Importance of nanofiber-matrix adhesion through SENT specimens with oriented nanofibers

Figure 10 shows the results in energy take-up for three different nanofiber orientations for both 6wt% PCL and 6wt% PA69 toughened specimens, i.e. randomly oriented (occurs naturally during electrospinning, referred to as *'random'*), aligned parallel to the tensile direction (referred to as *'0° aligned'*), and aligned perpendicular to the tensile direction (referred to as *'90° aligned'*).

We know from the previous section that the main toughness contribution occurs during crack growth, likely due to nanofiber bridging between the crack halves and an intensification of the FPZ. Hence, it is to be expected that the configuration with nanofibers aligned parallel to the tensile direction (*0° aligned*) would perform best as, in theory, each nanofiber immediately acts as a bridge between the crack halves. Yet, the results show an almost identical performance in energy take-up for the 0° aligned as well as the randomly oriented specimens. In-situ crack tip images of the 0° aligned specimens (**Figure 11** left) are also quite similar to those of the randomly oriented specimens (Figure 6). This indicates that in both cases, the majority of the nanofibers is effectively acting as a toughener by bridging. Indeed, due to the submicron scale of the nanofibers, the micron-

scale crack tip and the millimeter scale of the nanofiber bridging zone, the random orientation barely results in an effective loss of bridging nanofibers. This is also in agreement with the SEM image in Figure 7a taken just behind the crack tip of a specimen with randomly oriented nanofibers, where we see that many of the nanofibers are under an angle due to their initial random orientation in the electrospun veil, but are still effectively bridging the crack.

On the contrary, specimens with nanofibers aligned perpendicular to the tensile direction (*90° aligned*), show a decrease in energy take-up. Even more, PA69 nanofibers aligned 90° to the tensile direction even result in a more brittle fracture with a lot less energy take-up during initiation and propagation than the virgin material. The 6wt% PCL toughened specimens did still show an improvement in the crack propagation and total energy compared to the virgin material.

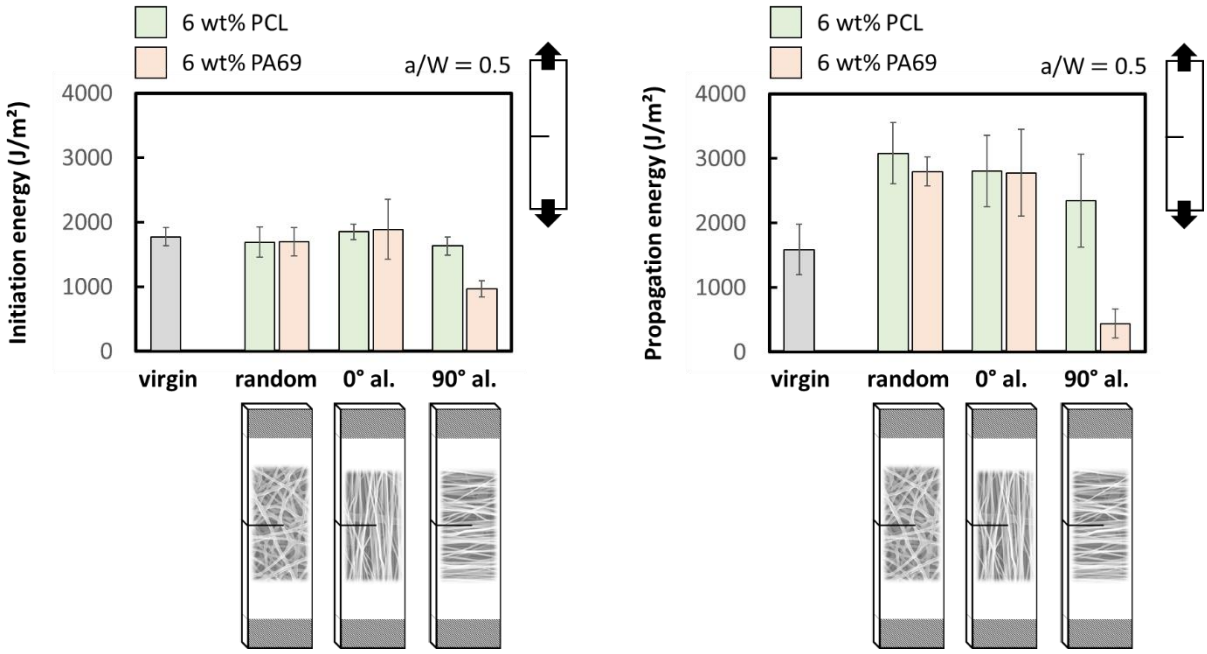

Figure 10 – Crack initiation (left) and propagation (right) energy for SENT specimens modified with 6wt% random, 0° aligned and 90° aligned PA69 and PCL nanofibers. For PCL modified specimens, the influence of nanofiber orientation is relatively low. On the other hand, a strong decrease in initiation and propagation energy is observed for 90° aligned PA69 nanofibers.

This can be explained by the difference in nanofiber/matrix adhesion for PCL and PA69 nanofibers. We know from previous studies that the PCL nanofibers adhere well to the RIMR135 epoxy system used here in comparison to PA nanofibers which debond from the matrix more easily [35,38]. This debonding mechanism is only a dominant factor when the nanofibers are aligned with the crack growth direction as in that case, the crack can progress by debonding. In turn, this will not result in an effective nanofiber bridging zone as the nanofibers can easily debond before they take up any substantial load. The in-situ crack tip images indeed confirm that while 90° aligned PCL toughened specimens still show quite some crack opening and nanofiber bridging, the 90° aligned PA69 toughened specimens show barely any crack opening nor nanofiber bridging (Figure 11).

The sensitivity of the SENT result to the nanofiber/matrix adhesion, where insufficient adhesion results in very large decreases of the energy take-up when the nanofibers are aligned with the crack growth direction, can be exploited. Indeed, these specimens could

serve as a direct measure of the interface quality to study nanofiber/matrix interactions in a relatively simple but sensitive way, instead of having to rely on indirect methods such as the delamination tests in Ref. [35,38].

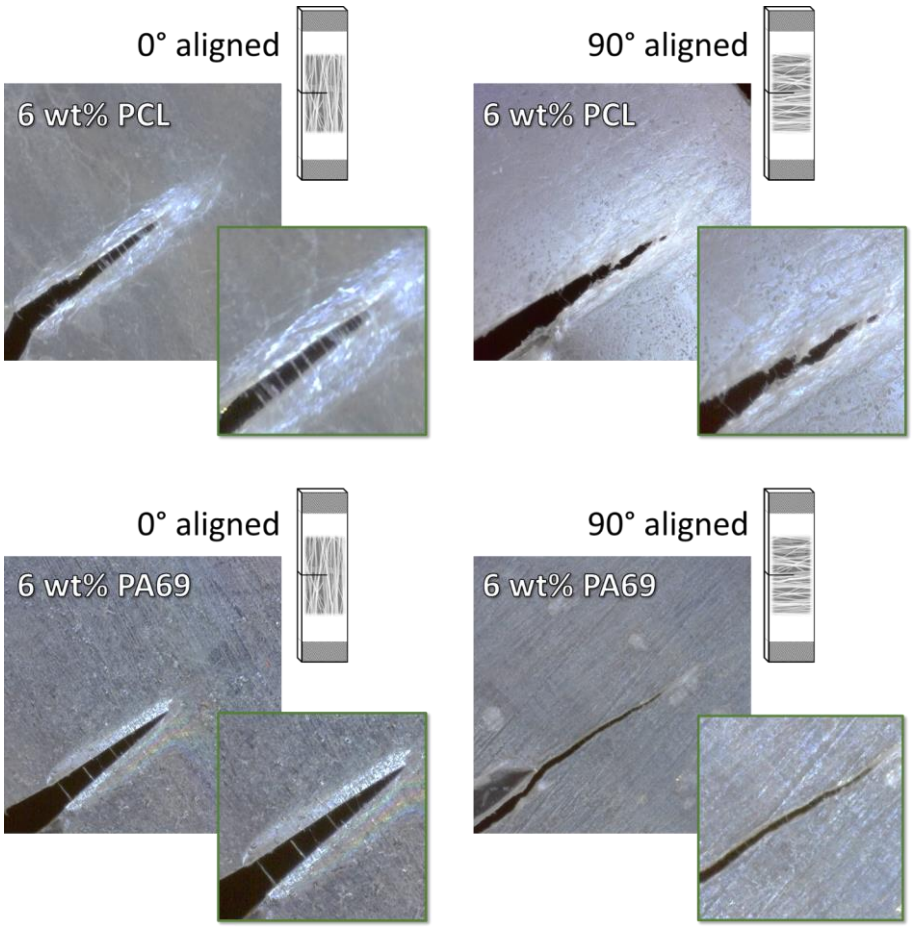

Figure 11 – In-situ view of the crack and nanofiber bridging zone just before the abrupt failure of 6wt% modified PCL and PA69 specimens with the nanofibers aligned parallel (left) and perpendicular (right) to the tensile direction. As evident from the energy take-up values, a big difference in the crack progression is observed for the 90° aligned PA69 nanofiber modified specimens, likely due to a lack of adhesion between the nanofibers and the epoxy matrix.

3.4. Contributions of the different toughening micro-mechanisms to the overall fracture behavior

Figure 12 gives a schematic summary of the different micro-mechanisms taking place during crack growth in a nanofiber toughened epoxy material, based on the results of the SENT experiments, in-situ microscopy of crack growth, SEM analysis of the crack halves and DIC analysis of the strain fields.

Behind the crack-tip, i.e. extrinsic toughening, the presence of bridging nanofibers creates crack-closing stresses in the crack halves, while the (plastic) elongation of the nanofibers under tensile loads is a major contribution to the increased energy take-up. Straining of the nanofibers predominantly happens behind the crack tip during bridging, as the strain values in front of the crack tip are limited (see Figure 8). The essential work of fracture w_f values found in the literature for bulk polyamides and polycaprolactone are between 10 – 60 kJ m^{-2} [48–50]. Hence, a rough estimation of the additional energy take-up due to nanofiber fracture ΔE_{nf} in the nanofiber modified specimens can be made as follows:

$$\Delta E_{nf} = vol\%_{nf}\left(w_{f,nf} - E_{tot,virgin}\right) \qquad \text{(Eq. 3)}$$

with volume percentage of nanofibers $vol\%_{nf}$, (essential) work of fracture of nanofibers $w_{f,nf}$ (in J m^{-2}) and the fracture energy for the virgin material $E_{tot,virgin}$ (in J m^{-2}). **Equation 3** represents the added work per unit fracture surface area taken-up assuming that the work $w_{f,nf}$ is done by the bridging nanofibers and the loss in work required to fracture the virgin matrix material due to less matrix material per unit fracture surface area. For the specimens considered here, this would result in an energy increase ranging from 400 J m^{-2} to 3400 J m^{-2}. This value corresponds well to the improvements reported in this work (approximately 500 – 2000 J m^{-2}) considering that factors such as debonding, nanofiber alignment and unstable crack growth are not taken into account. The high aspect ratio of nanofibers certainly favors the bridging toughening mechanism. The bridging nanofibers typically show a gradient with more intact fibers closer to the crack tip and more broken fibers further away from the crack tip. Near the boundaries of the crack halves, a plastically deformed region was visible as well. This region was produced in the intense plastic zone in front of the crack tip before crack progression.

The crack tip itself remains relatively sharp, indicating that crack initiation remains governed by the brittle epoxy, and induces a stress concentration field in the material.

In front of the crack tip (intrinsic toughening), one can expect micro-mechanisms such as nanofiber/matrix debonding, nanofiber straining and micro-cracking of matrix resin and nanofibers to be present, similar to traditional fiber-reinforced epoxy. These mechanisms all result in a large amount of "plasticity" visible at the millimeter scale in front of the crack tip. The strain fields obtained through DIC indeed confirmed that higher strains, and thus a more intense and larger plastic zone, are obtained for nanofiber modified specimens compared to the virgin material, resulting in a lower crack tip intensity. In addition, the crack closing stresses from the bridging nanofibers decrease the crack tip intensity as well. This is indeed confirmed by the longer stable crack growth region in the nanofiber modified specimens (Figure 4d).

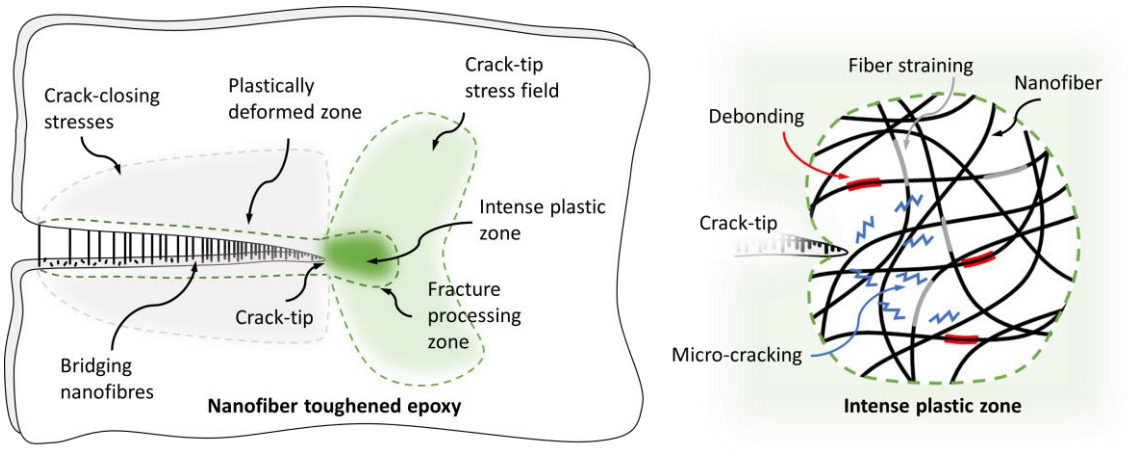

Figure 12 – Schematic representation of the toughening mechanisms acting inside a nanofiber modified epoxy.

The nanofiber bridging mechanism seems to match the well-known traditional fiber bridging mechanism present in carbon or glass fiber composites, with the distinction that the considered nanofibers are ductile in comparison to brittle glass or carbon fibers. To take up the most energy, as many nanofibers as possible should be bridging the crack halves. For example, using SENT specimens toughened with styrene-butadiene-styrene

electrospun microfibers that have a strain at break of over 800%, as used in Ref. [51,52] for the toughening of composite laminates, we see the development of a bridging zone without any broken fibers behind the crack tip (**Figure 13a**). However, depending on the (tensile) strain at break of the nanofibers themselves, a distinct gradient in the amount of bridging nanofibers is also observed with a very high bridging density at the crack tip and a decreasing amount of bridging nanofibers further behind the crack tip as more and more nanofibers reach their failure strain (**Figure 13b**). The strain at break and energy absorption at a certain strain (the area underneath the tensile stress-strain diagram) of the nanofibers are thus related to the toughening efficiency at a certain crack opening. When the strain at break is too high, the nanofibers will not be stretched until failure and will thus not absorb the maximal amount of energy. Similarly, the nanofibers' inherent toughness is important as it will determine the amount of energy absorbed at a certain strain. Furthermore, sufficient adhesion between the nanofibers and the epoxy ensures load transfer to the nanofibers, and thus bridging effects, even if they are aligned with the crack growth direction.

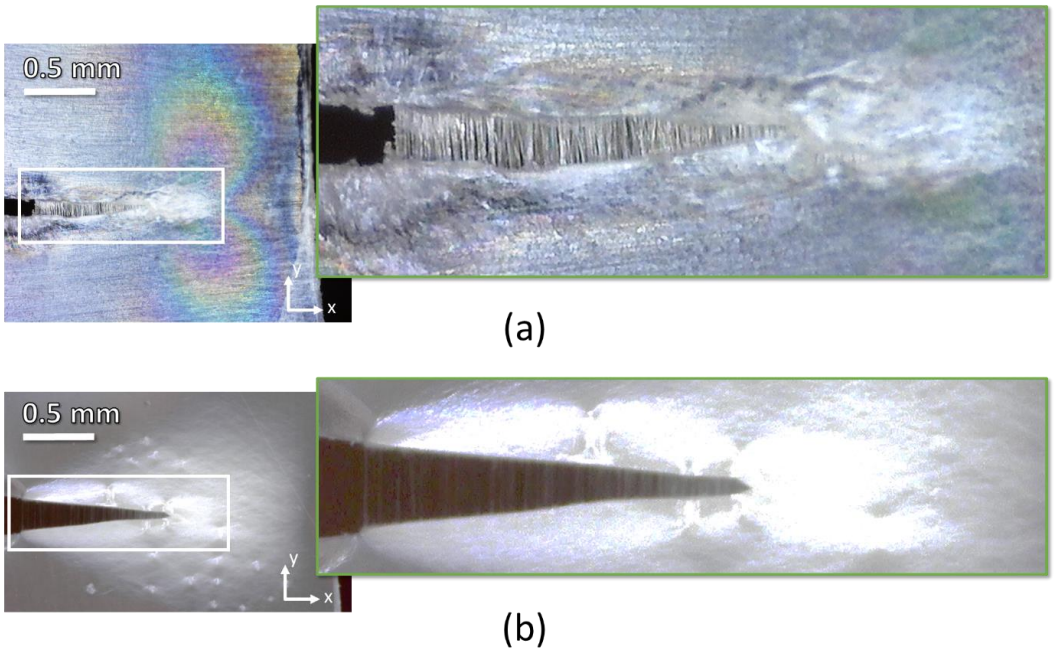

Figure 13 – (a) Fiber bridging zone in a modified SENT specimen using styrene-butadiene-styrene (SBS) "rubber" fibers with extremely high elongation does not show any broken fibers. (b) For PCL nanofibers, which have a lower strain at break than SBS fibers, a distinct gradient in bridging fiber density is observed. These results confirm the bridging mechanism and the tensile loading acting on the individual fibers upon crack opening.

4. Conclusions

Thermoplastic nanofibers are shown to be an effective toughener for epoxy materials. The addition of only 6 wt% PA69 or PCL nanofibers to the epoxy resin increased the fracture energy by 50 – 100%. Furthermore, the toughened epoxy materials showed longer stable crack lengths and continuously require more energy to grow cracks further (rising R-curve), making them inherently safer in for example structural applications.

Thanks to a film-like SENT specimen design, we determined the responsible micro-mechanisms that make the nanofibers such an effective toughener. In-situ optical and scanning electron microscopy during crack initiation and growth allowed to link the

occurrence of certain micro-mechanisms like nanofiber bridging to the load-displacement curves of the fracture tests.

In front of the crack tip, higher nominal strains are reached for nanofiber toughened epoxy, indicating a more intense fracture processing zone. In this zone, the nanofibers are still embedded in the surrounding epoxy matrix and experienced similar strains. Local debonding when the nanofiber/matrix interaction is insufficient and microcracking further result in larger-scale plasticity visible in front of the crack tip.

Behind the crack tip, nanofiber bridging, failure, and pull-out occurred during crack growth. Their occurrence coincided with the main increase in absorbed energy as determined by the load-displacement curves. The strain field behind the crack tip indicated the presence of crack-closing stresses due to bridging nanofibers as well as permanent plastic deformation due to a more intense fracture processing zone in comparison to untoughened epoxy specimens.

Using the insights obtained here, further optimizing of different nanofiber systems could be performed for applications ranging from high toughness coatings and adhesives to delamination resistant composite laminates.

5. Acknowledgments

Financial support from Research Foundation – Flanders (FWO) and Special Research Fund (BOF) Ghent University is gratefully acknowledged. Results in this paper were obtained within the framework of the FWO grant 12ZR520N, and the BOF BOFPDO2018000701 project.

6. Bibliography

[1] Turk M, Hamerton I, Ivanov DS. Ductility potential of brittle epoxies: Thermomechanical behaviour of plastically-deformed fully-cured composite resins. Polymer (Guildf) 2017;120:43–51. doi:10.1016/j.polymer.2017.05.052.

[2] Wisnom MR. The role of delamination in failure of fibre-reinforced composites. Philos Trans A Math Phys Eng Sci 2012;370:1850–70. doi:10.1098/rsta.2011.0441.

[3] He S, Shi K, Bai J, Zhang Z, Li L, Du Z, et al. Studies on the properties of epoxy resins modified with chain-extended ureas. Polymer (Guildf) 2001;42:9641–7. doi:10.1016/S0032-3861(01)00450-5.

[4] Jin Q, Misasi JM, Wiggins JS, Morgan SE. Simultaneous reinforcement and toughness improvement in an aromatic epoxy network with an aliphatic hyperbranched epoxy modifier. Polymer (Guildf) 2015;73:174–82. doi:10.1016/j.polymer.2015.07.031.

[5] Caldona EB, De Leon ACC, Pajarito BB, Advincula RC. A Review on Rubber-Enhanced Polymeric Materials. Polym Rev 2017;57:311–38. doi:10.1080/15583724.2016.1247102.

[6] Bagheri R, Marouf BT, Pearson RA. Rubber-toughened epoxies: A critical review. Polym Rev 2009;49:201–25. doi:10.1080/15583720903048227.

[7] Pearson RA, Yee AF. Toughening mechanisms in thermoplastic-modified epoxies: 1. Modification using poly(phenylene oxide). Polymer (Guildf) 1993;34:3658–70. doi:10.1016/0032-3861(93)90051-B.

[8] Marouf BT, Mai YW, Bagheri R, Pearson RA. Toughening of epoxy nanocomposites: Nano and hybrid effects. Polym Rev 2016;56:70–112. doi:10.1080/15583724.2015.1086368.

[9] Wang X, Jin J, Song M. An investigation of the mechanism of graphene toughening epoxy. Carbon N Y 2013;65:324–33. doi:10.1016/j.carbon.2013.08.032.

[10] Park YT, Qian Y, Chan C, Suh T, Nejhad MG, Macosko CW, et al. Epoxy Toughening with Low Graphene Loading. Adv Funct Mater 2015;25:575–85. doi:10.1002/adfm.201402553.

[11] Karapappas P, Vavouliotis A, Tsotra P, Kostopoulos V, Paipetis A. Enhanced Fracture Properties of Carbon Reinforced Composites by the Addition of Multi-Wall Carbon Nanotubes. J Compos Mater 2009;43:977–85. doi:10.1177/0021998308097735.

[12] Gojny FH, Wichmann MHG, Fiedler B, Schulte K. Influence of different carbon nanotubes on the mechanical properties of epoxy matrix composites - A comparative study. Compos Sci Technol 2005;65:2300–13. doi:10.1016/j.compscitech.2005.04.021.

[13] Huang Z-M, Zhang Y-Z, Kotaki M, Ramakrishna S. A review on polymer nanofibers by electrospinning and their applications in nanocomposites. Compos Sci Technol 2003;63:2223–53. doi:10.1016/S0266-3538(03)00178-7.

[14] Daelemans L, van der Heijden S, De Baere I, Rahier H, Van Paepegem W, De Clerck K. Damage resistant composites using electrospun nanofibers: a multiscale analysis of the toughening mechanisms. ACS Appl Mater Interfaces 2016;8. doi:10.1021/acsami.6b02247.

[15] Zheng N, Liu HY, Gao J, Mai YW. Synergetic improvement of interlaminar fracture energy in carbon fiber/epoxy composites with nylon nanofiber/polycaprolactone blend interleaves. Compos Part B Eng 2019;171:320–8. doi:10.1016/j.compositesb.2019.05.004.

[16] Ognibene G, Latteri A, Mannino S, Saitta L, Recca G, Scarpa F, et al. Interlaminar Toughening of Epoxy Carbon Fiber Reinforced Laminates: Soluble Versus Non-Soluble Veils. Polymers (Basel) 2019;11:1029. doi:10.3390/polym11061029.

[17] Di Filippo M, Alessi S, Palmese G, Dispenza C. Electrospun rubber/thermoplastic hybrid nanofibers for localized toughening effects in epoxy resins. J Appl Polym Sci 2019:48501. doi:10.1002/app.48501.

[18] Monteserín C, Blanco M, Murillo N, Pérez-Márquez A, Maudes J, Gayoso J, et al. Effect of different types of electrospun polyamide 6 nanofibres on the mechanical properties of carbon fibre/epoxy composites. Polymers (Basel) 2018;10. doi:10.3390/polym10111190.

[19] Neisiany RE, Khorasani SN, Naeimirad M, Lee JKY, Ramakrishna S. Improving Mechanical Properties of Carbon/Epoxy Composite by Incorporating Functionalized Electrospun Polyacrylonitrile Nanofibers. Macromol Mater Eng 2017;302:1600551. doi:10.1002/mame.201600551.

[20] Beylergil B, Tanoğlu M, Aktaş E. Enhancement of interlaminar fracture toughness of carbon fiber-epoxy composites using polyamide-6,6 electrospun

nanofibers. J Appl Polym Sci 2017;134:45244. doi:10.1002/app.45244.

[21] Palazzetti R, Zucchelli A. Electrospun nanofibers as reinforcement for composite laminates materials – A review. Compos Struct 2017;182:711–27. doi:10.1016/J.COMPSTRUCT.2017.09.021.

[22] Brugo T, Minak G, Zucchelli A, Yan XT, Belcari J, Saghafi H, et al. Study on Mode I fatigue behaviour of Nylon 6,6 nanoreinforced CFRP laminates. Compos Struct 2017;164:51–7. doi:10.1016/j.compstruct.2016.12.070.

[23] Beckermann GW, Pickering KL. Mode I and Mode II interlaminar fracture toughness of composite laminates interleaved with electrospun nanofibre veils. Compos Part A Appl Sci Manuf 2015;72:11–21. doi:10.1016/j.compositesa.2015.01.028.

[24] Daelemans L, Cohades A, Meireman T, Beckx J, Spronk S, Kersemans M, et al. Electrospun nanofibrous interleaves for improved low velocity impact resistance of glass fibre reinforced composite laminates 2018;141:170–84.

[25] Wu X-FF, Rahman A, Zhou Z, Pelot DD, Sinha-Ray S, Chen B, et al. Electrospinning core-shell nanofibers for interfacial toughening and self-healing of carbon-fiber/epoxy composites. J Appl Polym Sci 2013;129:1383–93. doi:10.1002/app.38838.

[26] Dong Y, Li S, Zhou Q. Self-healing capability of inhibitor-encapsulating polyvinyl alcohol/polyvinylidene fluoride coaxial nanofibers loaded in epoxy resin coatings. Prog Org Coatings 2018;120:49–57. doi:10.1016/j.porgcoat.2018.03.010.

[27] Doan TQ, Leslie LS, Kim SY, Bhargava R, White SR, Sottos NR. Characterization of core-shell microstructure and self-healing performance of electrospun fiber coatings. Polymer (Guildf) 2016;107:263–72.

[28] Li J, Hu Y, Qiu H, Yang G, Zheng S, Yang J. Coaxial electrospun fibres with graphene oxide/PAN shells for self-healing waterborne polyurethane coatings. Prog Org Coatings 2019;131:227–31. doi:10.1016/j.porgcoat.2019.02.033.

[29] Lee MW, An S, Lee C, Liou M, Yarin AL, Yoon SS. Self-healing transparent core-shell nanofiber coatings for anti-corrosive protection. J Mater Chem A 2014;2:7045–53. doi:10.1039/c4ta00623b.

[30] Ekrem M, Avcı A. Effects of polyvinyl alcohol nanofiber mats on the adhesion strength and fracture toughness of epoxy adhesive joints. Compos Part B Eng 2018;138:256–64. doi:10.1016/j.compositesb.2017.11.049.

[31] Razavi SMJ, Neisiany RE, Ayatollahi MR, Ramakrishna S, Khorasani SN, Berto F. Fracture assessment of polyacrylonitrile nanofiber-reinforced epoxy adhesive. Theor Appl Fract Mech 2018;97:448–53. doi:10.1016/j.tafmec.2017.07.023.

[32] On SY, Kim MS, Kim SS. Effects of post-treatment of meta-aramid nanofiber mats on the adhesion strength of epoxy adhesive joints. Compos Struct 2017;159:636–45. doi:10.1016/j.compstruct.2016.10.016.

[33] Daelemans L, van der Heijden S, De Baere I, Rahier H, Van Paepegem W, De Clerck K. Improved fatigue delamination behaviour of composite laminates with electrospun thermoplastic nanofibrous interleaves using the Central Cut-Ply method. Compos Part A Appl Sci Manuf 2017;94:10–20. doi:10.1016/j.compositesa.2016.12.004.

[34] van der Heijden S, Daelemans L, Meireman T, De Baere I, Rahier H, Van Paepegem W, et al. Interlaminar toughening of resin transfer molded laminates by electrospun polycaprolactone structures: Effect of the interleave morphology. Compos Sci Technol 2016;136:10–7. doi:10.1016/j.compscitech.2016.09.024.

[35] Daelemans L, Kizildag N, Van Paepegem W, D'hooge DR, De Clerck K. Interdiffusing core-shell nanofiber interleaved composites for excellent Mode I and Mode II delamination resistance. Compos Sci Technol 2019;175:143–50. doi:10.1016/J.COMPSCITECH.2019.03.019.

[36] van der Heijden S, Daelemans L, De Schoenmaker B, De Baere I, Rahier H, Van Paepegem W, et al. Interlaminar toughening of resin transfer moulded glass fibre epoxy laminates by polycaprolactone electrospun nanofibres. Compos Sci Technol 2014;104:66–73. doi:10.1016/j.compscitech.2014.09.005.

[37] Daelemans L, van der Heijden S, De Baere I, Rahier H, Van Paepegem W, De Clerck K. Using aligned nanofibres for identifying the toughening micromechanisms in nanofibre interleaved laminates. Compos Sci Technol 2016;124:17–26. doi:10.1016/j.compscitech.2015.11.021.

[38] Daelemans L, Van Paepegem W, D'hooge DR, De Clerck K. Excellent Nanofiber Adhesion for Hybrid Polymer Materials with High Toughness Based on Matrix Interdiffusion During Chemical Conversion. Adv Funct Mater 2018:1807434. doi:10.1002/adfm.201807434.

[39] Daelemans L, van der Heijden S, De Baere I, Muhammad I, Van Paepegem W, Rahier H, et al. Bisphenol A based polyester binder as an effective interlaminar toughener. Compos Part B Eng 2015;80:145–53. doi:10.1016/j.compositesb.2015.05.044.

[40] Giannakopoulos I, Taylor AC. An essential work of fracture study of the toughness of thermoset polyester coatings. Prog Org Coatings 2015;78:265–74. doi:10.1016/j.porgcoat.2014.08.009.

[41] Yang JL, Zhang Z, Zhang H. The essential work of fracture of polyamide 66 filled with TiO2 nanoparticles. Compos Sci Technol 2005;65:2374–9. doi:10.1016/j.compscitech.2005.06.008.

[42] Hashemi S. Determination of the fracture toughness of polybutylene terephthalate (PBT) film by the essential work method: Effect of specimen size and geometry. Polym Eng Sci 2000;40:798–808. doi:10.1002/pen.11209.

[43] Karger-Kocsis J, Ferrer-Balas D. On the plane-strain essential work of fracture of polymer sheets. Polym Bull 2001;46:507–12. doi:10.1007/s002890170039.

[44] Bárány T, Czigány T, Karger-Kocsis J. Application of the essential work of fracture (EWF) concept for polymers, related blends and composites: A review. Prog Polym Sci 2010;35:1257–87. doi:10.1016/j.progpolymsci.2010.07.001.

[45] Allaer K, De Baere I, Van Paepegem W, Degrieck J. Direct fracture toughness determination of a ductile epoxy polymer from digital image correlation measurements on a single edge notched bending sample. Polym Test 2015;42:199–207. doi:10.1016/j.polymertesting.2015.01.014.

[46] Daelemans L, van der Heijden S, De Baere I, Rahier H, Van Paepegem W, De Clerck K. Nanofibre bridging as a toughening mechanism in carbon/epoxy composite laminates interleaved with electrospun polyamide nanofibrous veils.

Compos Sci Technol 2015;117:244–56. doi:10.1016/j.compscitech.2015.06.021.

[47] Bilge K, Yorulmaz Y, Javanshour F, Ürkmez A, Yılmaz B, Şimşek E, et al. Synergistic role of in-situ crosslinkable electrospun nanofiber/epoxy nanocomposite interlayers for superior laminated composites. Compos Sci Technol 2017;151:310–6. doi:10.1016/J.COMPSCITECH.2017.08.029.

[48] Ludueña LN, Stocchi A, Alvarez VA. Fracture behavior of polycaprolactone/clay nanocomposites. J Compos Mater 2016;50:3863–72. doi:10.1177/0021998315626505.

[49] Wong SC, Baji A, Gent AN. Effect of specimen thickness on fracture toughness and adhesive properties of hydroxyapatite-filled polycaprolactone. Compos Part A Appl Sci Manuf 2008;39:579–87. doi:10.1016/j.compositesa.2007.09.004.

[50] Yamakawa RS, Razzino CA, Correa CA, Hage E. Influence of notching and molding conditions on determination of EWF parameters in polyamide 6. Polym Test 2004;23:195–202. doi:10.1016/S0142-9418(03)00080-1.

[51] van der Heijden S, Daelemans L, De Bruycker K, Simal R, De Baere I, Van Paepegem W, et al. Novel composite materials with tunable delamination resistance using functionalizable electrospun SBS fibers. Compos Struct 2017;159:12–20. doi:10.1016/j.compstruct.2016.09.057.

[52] van der Heijden S, De Bruycker K, Simal R, Du Prez F, De Clerck K. Use of Triazolinedione Click Chemistry for Tuning the Mechanical Properties of Electrospun SBS-Fibers. Macromolecules 2015;48:6474–81. doi:10.1021/acs.macromol.5b01569.